Ceramics International 43 (2017) 1354–1361

Contents lists available at ScienceDirect

Ceramics International

journal homepage: www.elsevier.com/locate/ceramint

Influence of the substrate gas-inlet gap on the growth rate, morphology and microstructure of zirconium carbide films grown by chemical vapour deposition

S. Biira[a,b,*], B.A.B. Alawad[a], H. Bissett[c], J.T. Nel[c], T.P. Ntsoane[d], T.T. Hlatshwayo[a], P.L. Crouse[e], J.B. Malherbe[a]

[a] Department of Physics, University of Pretoria, Pretoria 0002, South Africa
[b] Department of Physics, Busitema University, P.O. Box 236, Tororo, Uganda
[c] Applied Chemistry Division, The South African Nuclear Energy Corporation (Necsa), P.O. Box 582, Pretoria 0001, South Africa
[d] Radiation Science Division, The South African Nuclear Energy Corporation (Necsa), P.O. Box 582, Pretoria 0001, South Africa
[e] Department of Chemical Engineering, University of Pretoria, 0002, South Africa

ARTICLE INFO

Keywords:
Microstructure
Zirconium carbide films
Growth rate
Chemical vapour deposition
XRD

ABSTRACT

The influence of the gap between the gas inlet and the substrate in an in-house developed thermal chemical vapour deposition (CVD) reactor, on the growth rate, surface morphology, phase composition and microstructure of deposited ZrC films was investigated by X-ray diffraction (XRD) and scanning electron microscopy (SEM). The ZrC films were grown on high density graphite substrates at different substrate-inlet gaps, viz. 70 mm, 90 mm, 120 mm, 145 mm and 170 mm, at substrate temperatures of 1200 °C and 1400 °C. The growth rate of ZrC films prepared at 1400 °C was observed to be higher than at 1200 °C., and was found to decrease with increase in substrate-inlet gap at both temperatures. The boundary layer thickness increased with an increase in substrate-inlet gap. The diffusion coefficients of the reactants were found to be 0.176 cm^2/s and 0.200 cm^2/s for the ZrC films deposited at 1200 °C and 1400 °C respectively. A model illustrating the diffusion of source materials through the boundary layer to the reacting surface was also given. The XRD results of ZrC films showed that at both 1200 °C and 1400 °C the (111) plane was the less preferred orientation, while (200) and (220) were the preferred planes. The degree of preferred orientation of ZrC films was found to decrease with increasing substrate-inlet gap. SEM results indicated that as the substrate-inlet gap increased from 70 mm to 170 mm for 1400 °C, the films became more uniform with increased particle agglomeration. The cauliflower-like clusters of particles grew larger in size and covered the whole surface. By contrast, at 1200 °C the surface crystallites had complex facets that decreased in size as the substrate-inlet gap increased from 70 mm to 170 mm.

1. Introduction

Owing to its excellent physical properties, zirconium carbide (ZrC) has been proposed as a possible new material to be used as a protective coating layer for *TRISO* (Tristructural-isotropic) nuclear fuel particle [1–3]. These properties include: high melting temperature (about 3540 °C), low density (6.59 g/cm^3) compared to other refractory carbides, chemical inertness to various reagents and high wear and corrosion resistance [1,3]. Many attempts have been made to grow ZrC films.

Several techniques such as plasma spraying [4], sol gel synthesis [5,6], carbothermal reduction [7], magnetron sputtering [8], reactive melt infiltration [9] and chemical vapour deposition (CVD) [10–12], have been used to produce ZrC. However, growing polycrystalline ZrC films with good stoichiometry has remained a challenge. When the deposition conditions are well managed, CVD produces ZrC films with relatively low levels of impurity and porosity [13]. This has made CVD the most suitable technique for growing multilayer coatings. The ZrC film parameters such as growth rate, surface morphology, stoichiometry, crystallite size, texture, structural defects and porosity are influenced by the CVD reactor geometry and deposition conditions [14]. This is because the reaction rates and mass transport of the inlet gases in the reaction chamber and on the substrate surface are governed by kinetics which depend on both reactor geometry and process para-

* Corresponding author at: Department of Physics, University of Pretoria, Pretoria 0002, South Africa.
E-mail address: bsaphina@yahoo.co.uk (S. Biira).

http://dx.doi.org/10.1016/j.ceramint.2016.10.092
Received 20 August 2016; Received in revised form 24 September 2016; Accepted 14 October 2016
Available online 18 October 2016

meters [15]. Chemical vapour deposition of materials carried out at atmospheric pressure operate in a mass transport-limited mode [14]. Therefore reactor and flow geometries are crucial for the film characteristics and growth rate [15]. Hence to produce ZrC films with good properties, deposition geometry and technique should be well managed.

During the course of our experimental work, it became evident that the position of the reactive gas inlet above the substrate had a distinct and unexpected effect on the growth parameters of ZrC. This possibility has been mentioned before in a computational study by Vanka et al. [16]. They noted that the gap between the substrate and the inlet is a sensitive parameter since it determines the natural convection parameters and therefore affects growth dynamics of the coatings [16]. To our knowledge, no experimental work has been reported on the growth and properties of ZrC films in an induction heated CVD reactor at different substrate-gas inlet gaps. This study reports the influence of substrate-gas inlet gap on the growth rate, surface morphology and microstructure of ZrC films deposited on graphite substrates. The experimental work was performed in an atmospheric pressure induction heated graphite vertical wall CVD reactor using a $ZrCl_4/CH_4/H_2$/Ar gas mixtures with the gas composition and flow rates held constant. Lui et al. [10] noted that the deposition process of ZrC films is controlled by gas nucleation at substrate temperature below 1250 °C and by surface reaction kinetics at substrate temperature above 1250 °C. For this reason the temperature of substrate temperatures of 1200 °C and 1400 °C were selected for this work.

2. Experimental

2.1. Apparatus

ZrC films were deposited on graphite substrates using an inductively-heated vertical CVD system which was developed in-house at Necsa shown in Fig. 1. The vertical graphite reaction chamber of 300 mm long with an internal diameter of 25 mm was used. The graphite substrate stage, with a diameter of 23 mm, was fixed at the bottom of the reaction chamber. Two graphite substrates, each with a 10 mm diameter and 2.5 mm thick, were positioned on top of the substrate stage. The substrates were placed in such a way that the surface to be deposited on, was perpendicular to the gas feed line. A water-cooled tubular copper induction coil wound close to the exterior wall of the graphite reaction chamber was used as heat source.

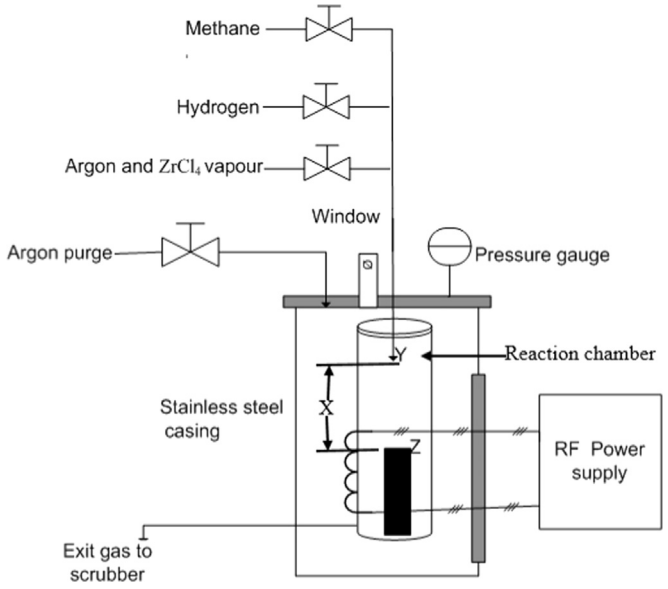

Fig. 1. Schematic diagram of the CVD reactor system.

The substrate-gas inlet gap (ZY) (see Fig. 1) was varied from 70 mm to 90 mm, 120 mm, 145 mm and 170 mm. This was done by changing the inlet (Y) feed line lengths and maintaining the substrates at the same position on the top of the substrate stage (Z). Changing the substrate position would result in changes to the temperature of the substrate and its immediate vicinity since the temperature at any point inside the reactor is dependent on its position relative to the induction heating coil. Prior to the start of deposition, the reaction chamber was flushed with argon by pressurising and depressurising five times. A rotary vane vacuum pump (not indicated in Fig. 1) connected to the extraction line was used to pump away the argon and regulate the pressure in the reaction chamber during deposition. The process and instrumentation diagram is illustrated in [17].

Anhydrous $ZrCl_4$ powder (purity > 99.5%, Hf < 50 mg/kg) supplied by Sigma–Aldrich and methane (purity > 99.999%) were respectively used as zirconium and carbon precursors for the deposition of ZrC films. Hydrogen gas was used to provide a reducing environment for $ZrCl_4$ and to dilute the HCl effluent. The ZrC deposition process may be described by the overall chemical reaction given by Eq. (1).

$$ZrCl_4(g) + CH_4(g) \rightarrow ZrC(s) + 4HCl(g) \quad (1)$$

The $ZrCl_4$ powder was maintained at a temperature of 300 °C in order to control its vapour pressure. The $ZrCl_4$ vapour was then swept into the reaction chamber by argon carrier gas. The $ZrCl_4$ mass transfer rate to the rector was controlled by regulating the argon carrier flow rate. The flow rates of argon, hydrogen and methane were controlled by manual flow meters. The deposition was conducted at atmospheric pressure at two substrate temperatures viz. 1200 °C and 1400 °C for 2 h. The deposition parameters are indicated in Table 1.

2.2. Characterisation of ZrC films

The crystal structure, phase composition, and the preferred orientations of the films were determined by X-ray diffraction (XRD) using a Bruker D8 Advance diffractometer with Cu K_α (λ=0.15418 nm) radiation. Diffracted data was collected using a LynxEye position sensitive detector. The phase composition of the films from the XRD patterns was analysed by the Rietveld refinement method using the TOPAS V4.2 [18] software package. The surface morphology of as deposited ZrC films was analysed using ultrahigh resolution field-emission scanning electron microscopy (FE-SEM, Zeiss Ultra Plus) with working voltage set at 1 kV.

3. Results and discussions

3.1. Gas flow parameters in the reaction chamber

It was assumed that the total reactant gas pressure was uniform throughout the reactor space for the entire deposition time and the reactants did not react chemically in vapour phase to form ZrC. Some of the gas properties are indicated in Table 1.

Table 1
Experimental growth parameters for ZrC films.

Time (h)	Pressure (atm)	Substrate temperature (°C)	Substrate-gas inlet gap (mm)	Vapouriser temperature (°C)
2	1.0	1200 and 1400	70–170	300
Gases	**Flow rate Q_i (sccm)**	**Velocity V_i (m/s)**	**Density ρ_i (kg/m^3)**	**Viscosity×10^{-5} η_i (Pa.s)**
CH_4	26	0.442	0.6669 at 20 °C	1.1 at 20 °C
H_2	853	0.0135	0.0838 at 20 °C	0.88 at 20 °C
Ar	562	0.291	0.8494 at 300 °C	3.67 at 300 °C

The velocity V of the mixture of gases entering the reaction chamber was calculated using Eq. (2).

$$V = \frac{\sum_i \rho_i V_i}{\sum_i \rho_i} \tag{2}$$

where ρ_i and V_i are the density and velocity of the i^{th} component respectively with $V_i = Q_i/(60\pi r^2)$ and r (0.32 cm) being the radius of the inlet steel pipes. The velocity V of the gas mixture was found to be 0.183 m/s.

The values of density, velocity and viscosity of $ZrCl_4$ vapour was not included in the calculations since $ZrCl_4$ vapour constituted the smallest (and negligible) fraction of the total gas mixture. The density of the gas mixture was estimated from Eq. (3) and was found to be 0.393 kg/m^3.

$$\rho = \frac{\sum_i \rho_i Q_i}{\sum_i Q_i} \tag{3}$$

The viscosity of the gas mixture was calculated from Eq. (4).

$$\eta = \frac{\sum_i y_i \eta_i \sqrt{M_i}}{\sum_i y_i \sqrt{M_i}} \tag{4}$$

where y_i, M_i and η_i are the mole fraction, molar weight and viscosity respectively of the i^{th} component at the desired temperature. The mole fraction of an individual gas was determined from their volumetric flow rates as $y_i = Q_i/\sum_i Q_i$ [13]. The viscosity of the gas mixture was found to be 2.92×10^{-5} Pa s.

The growth of ZrC films on the substrate is controlled by $ZrCl_4/CH_4$ diffusion to the surface of the substrate. Assuming the concentration of $ZrCl_4/CH_4$ in the vicinity of the substrate surface tends towards zero, then the concentration drop between the bulk and the surface is equal to the inlet concentration N_o. The concentration of individual reactants in the mixture was calculated from Eq. (5).

$$N_o = \frac{w_i \dot{m}_i}{M_i Q_i} \tag{5}$$

where $\dot{m}_i$ is the reactant mass transfer rate and w_i is the molar fraction. In this study, the $ZrCl_4$ concentration in the mixture was found to be 8.12×10^{-8} mol/cm^3. The molecular volume of the growing ZrC layer v_k is 15.67 cm^3/mol.

From the experimental parameters and gas properties, the Reynold's number (Re) at the inlet inside the reaction chamber was found to be 61.7, indicating that the flow of the reactants in the reaction chamber was mainly laminar. The Reynold's number was determined from Eq. (6).

$$\mathrm{Re} = \frac{V\rho d}{\eta} \tag{6}$$

where d=2.5 cm is the diameter of the reaction chamber.

Due to natural convection and the friction between the reactant flow and the substrate surface (viscosity of the reactants), the velocity of the reactants in the vicinity of the substrate surface reaches a minimum. The difference in the gas flow velocities at the substrate surface and the bulk gives rise to a stagnant boundary layer. The boundary layer thickness δ is related to the Reynold's number by Eq. (7) [19].

$$\delta = \sqrt{X}\sqrt{\frac{d}{\mathrm{Re}}} \tag{7}$$

The boundary layer thickness was estimated to be 5.3 mm, 6.0 mm, 7.0 mm, 7.8 mm and 8.3 mm for substrate inlet gap X equal to 70 mm, 90 mm, 120 mm, 145 mm and 170 mm respectively.

3.2. Growth rate

The change in film thickness per unit deposition time (i.e. the growth rate, k) was determined from Eq. (8).

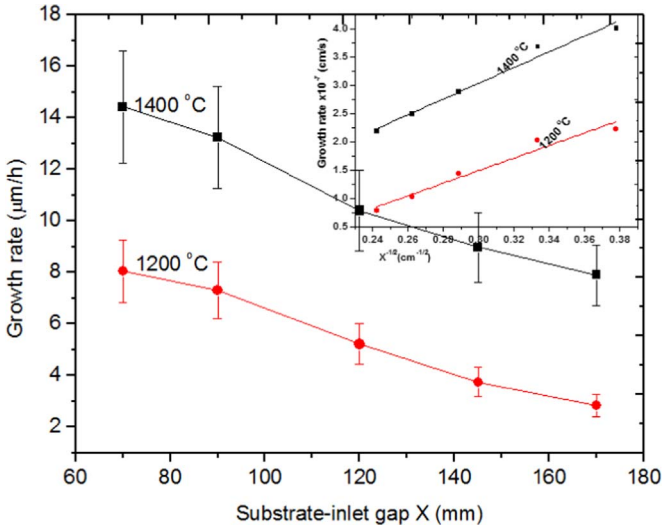

Fig. 2. The plot showing the dependence of growth rate of ZrC films on substrate-inlet gap X. the insert shows the growth rate as a function of the reciprocal of the square root of X.

$$k = \frac{M}{tA\rho_{ZrC}} \tag{8}$$

where m is the mass of the film, $A$is the surface area of the substrate, ρ_{ZrC} (6.59 g/cm^3) is the theoretical density of ZrC and t is the deposition time. The deposition time was considered as the duration which the precursors flowed into the reactor.

The effect of substrate-inlet gap and substrate temperature on the growth rate of ZrC films is shown by Fig. 2. From these plots, it is quite clear that the growth rate decreases almost linearly with increase in substrate–inlet gap at both temperatures. The results also show an increased growth rate when the temperature is increased from 1200 °C to 1400 °C. The effect of the gas inlet position may be due to increased diffusion rate of reactant species across the boundary layer [20] and the temperature effect may be due to increased surface reaction kinetics at higher temperatures [21]. The transport of the reactants in the reaction chamber is controlled by complex fluid dynamics [19,22]. The detailed examination of fluid dynamics in the vertical wall CVD is not presented in this work. We shall limit our discussion to diffusion of the reactants through the boundary layer. The boundary layer give rise to changes in the reactant flow velocity which results in a concentration gradient of reactant gases in the vicinity of the substrate surface [19,23]. The reactant gas concentration in the vicinity of the substrate surface is usually higher when the gas inlet is closer to the substrate. The higher gas concentration results in an increased mass transfer rate and this increases the arrival rates of reacting species to the substrate surface. The flux J of the reactant through the boundary layer in the vicinity of the substrate surface inside the reaction chamber is given by Eq. (9).

$$J = \frac{-DN_0}{\delta} \tag{9}$$

where D is diffusion constant (a proportionality constant between the molar flux due to molecular diffusion and the gradient in concentration of the reactant species) and N_o is the concentration difference over the boundary layer thicknessδ[23]. Therefore increasing the boundary layer thickness reduces the diffusion flux of the reactants. The growth rate k, in terms of diffusion flux, boundary layer thickness and substrate–inlet gap is expressed by Eq. (10).

$$k = -v_k J = \left(v_k D N_0 \sqrt{\frac{\mathrm{Re}}{d}}\right)\frac{1}{\sqrt{X}} \tag{10}$$

where v_k is the molecular volume of the crystal [27]. This expression shows that the growth rate is determined by the reciprocal of the

square root of the substrate-inlet gap. This is in agreement with our experimental results obtained in Fig. 2, where the growth rate is observed to have a linear relationship to the reciprocal of the square root of substrate-inlet gap.

It was also observed (by visual inspection) that when the substrate–inlet gap was wide (short inlet feed line), the amount of $ZrCl_4$ gas diffusing out of the reaction chamber increased and deposited on the top lid of the stainless-steel casing. This might have decreased the concentration of $ZrCl_4$ reaching the substrate and consequently contributed to decrease in ZrC film growth rate as substrate-inlet gap increased.

From the slope of the curves in the insert in Fig. 2 (1.111×10^{-6} $cm^{-3/2}$ for 1200 °C and 1.393×10^{-6} $cm^{-3/2}$ for 1400 °C) and the parameters of the multicomponent reactant gaseous mixture indicated in Section 3.1, the diffusion coefficients of the reactants for ZrC films growth process were determined from Eq. (11).

$$D = \left(\sqrt{\frac{d}{\mathrm{Re}}}\right)\frac{slope}{v_k N_0} \tag{11}$$

The reactant diffusivity was found to be 0.176 cm^2/s and 0.200 cm^2/s for 1200 °C and 1400 °C respectively. These values show that the derived diffusion coefficients increase marginally as the substrate temperature is increased. The values of diffusion coefficients above are likely to be low, since they are determined from the actual growth rate of the films, and yet not all the diffusing reactants are effectively used to form the ZrC film. The reactant loss may arise from parasitic reactions inside the reaction chamber and the reactants diffusing out of the chamber unreacted.

To explain the deposition mechanism, we use a concentration boundary layer model given in Fig. 3. A number of steps are involved in the growth process; (1) The inlet gases ($ZrCl_4$ in Ar, CH_4 and H_2) are transported to the heated substrate surface or boundary layer, (2) gas phase reactions take place and the intermediate species (i.e. CH_4=C +2H_2) which form are transported (diffuse) through the boundary layer to the substrate, (3) the reactants and their intermediate species diffuse and are absorbed into the heated substrate surface. This produces the ZrC deposit and by-products, (4) the ZrC deposit then diffuse along the heated substrate surface forming crystallisation centres leading to the growth of the ZrC film according to the Burton-Cabrera-Frank step-flow mechanism [29]. In parallel with this, (5) the by-products and unreacted reactants are removed from the deposited film surface by convection, (6) some reactants and their intermediate product are lost within and from the reaction chamber, and (7) the by-products and unreacted reactants are transported away from the reaction chamber. The slowest process determines the actual film growth rate. For the deposition conditions and parameters used in this work, mass transport (diffusion) across the boundary layer becomes the rate controlling step.

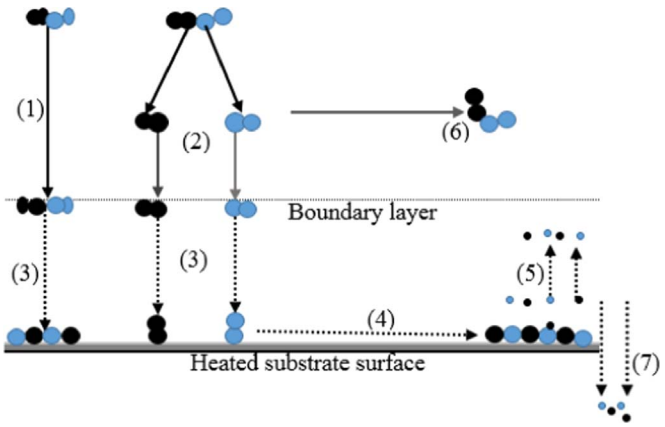

Fig. 3. Concentration boundary layer model for CVD process of ZrC films in the vertical reaction chamber.

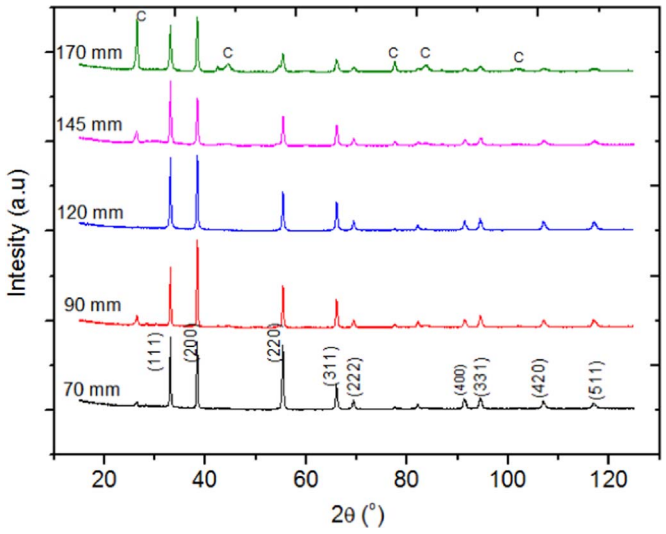

Fig. 4. XRD patterns of ZrC films deposited at 1200 °C for different substrate-inlet gaps.

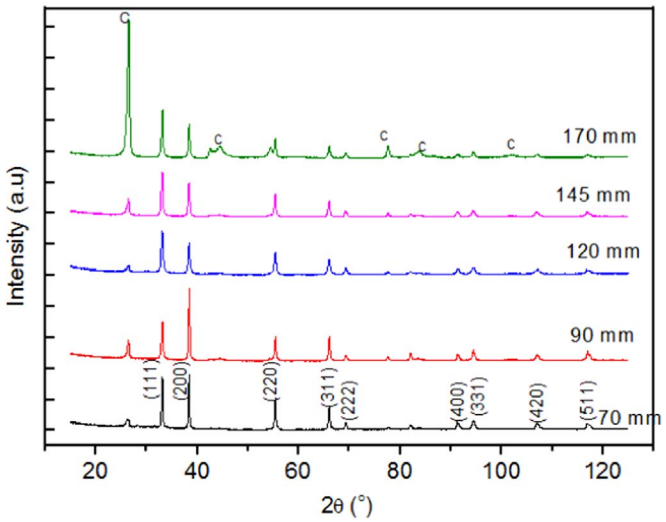

Fig. 5. XRD patterns of ZrC films deposited at 1400 °C for different substrate-inlet gaps.

3.3. Crystallographic structure and phase composition

The crystal structure and phase composition of all the deposited ZrC films were investigated by XRD analysis. Figs. 4 and 5 show the XRD patterns of ZrC films deposited at 1200 °C and 1400 °C respectively. The peaks and their corresponding Miller indices are also indicated in the figures. The diffraction peaks present were indexed within a cubic rock salt (NaCl) structure and confirmed using the International Centre for Diffraction Data (ICDD) file number ZrC: 03-065-8833. Carbon peaks (matched with ICCD file number C: 00-056-0159) are evident in XRD patterns as shown by Figs. 4 and 5. The carbon peak intensities were observed to increase with both substrate-inlet gap increase (from 70 mm to 170 mm) and temperature increase (from 1200 °C to 1400 °C). Phase quantification was performed by Rietveld refinement [30]. The results revealed that the samples consisted mainly of the ZrC phase and some amounts of free carbon. The C/ZrC ratios at the two temperatures for each substrate-inlet gap was determined and plotted as shown in Fig. 6. At 1200 °C the C/ZrC ratio is lower than at 1400 °C for all the substrate-inlet gaps. The figure also shows a general increase of C/ZrC ratio with increase in substrate-inlet gaps. The increase in free carbon may be attributed to the fact that the rate at which methane decomposes to form carbon and hydrogen

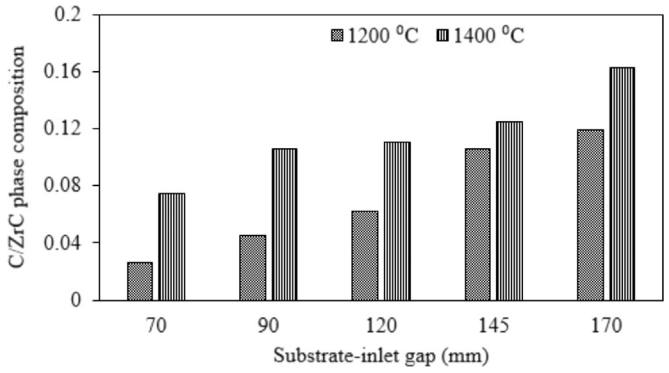

Fig. 6. C/ZrC phase composition as a function of substrate-inlet gap.

increases with increasing temperature; higher growth rates imply higher fluxes of reactants to the deposition surface, and a higher probability for methane to decompose rather than to take part in a concerted reaction to form the carbide. Generally the diffusion rate of heavy gas molecules is lower compare to the light gas molecules and this corresponds to their participation in the growth process. When the substrate-inlet gap is narrowed, $ZrCl_4$ is brought closer to the substrate and its participation in the growth process is improved, hence C/ZrC decreases.

3.4. Crystallite size

The crystallite size of polycrystalline materials affects their mechanical properties [31]. Average crystallite size can be calculated from the Scherrer formula:

$$D = \frac{0.94\lambda}{B\cos\theta} \tag{12}$$

where λ is the X-ray wavelength (0.15418 nm), B is the full width at half maximum (FWHM) of a given diffraction peak, and θ is the Bragg angle [30].

Fig. 7 illustrates the dependence of average crystallite size of ZrC films on substrate-inlet gap at 1200 °C and 1400 °C. The average crystallite size decreased from 33.3 ± 0.8 nm to 22.8 ± 1.0 nm for ZrC films deposited at 1200 °C and from 30.8 ± 0.2 nm to 21.2 ± 0.6 nm for films deposited at 1400 °C as the substrate-inlet gap increased from 70 mm to 170 mm. This reduction in average crystallite size might be due to two reasons. The reduced reactant concentrations at the substrate surface at wider substrate-inlet gaps may retard crystallite growth. Furthermore, as indicated in Fig. 6, the increase in substrate-inlet gap results in an increase in the amount of free carbon. This free carbon, which is deposited as a secondary phase, acts as an impurity in the deposited film. The presence of carbon impurities in the ZrC films may also cause retardation in the crystallite growth.

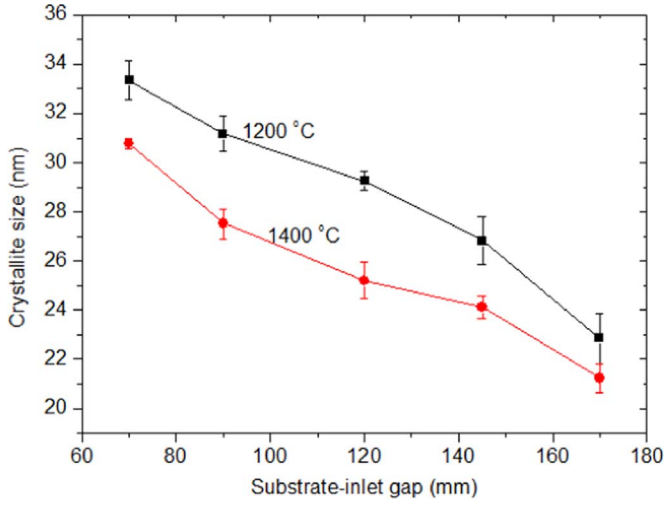

Fig. 7. Average crystallite size of ZrC films dependence on substrate-inlet gap.

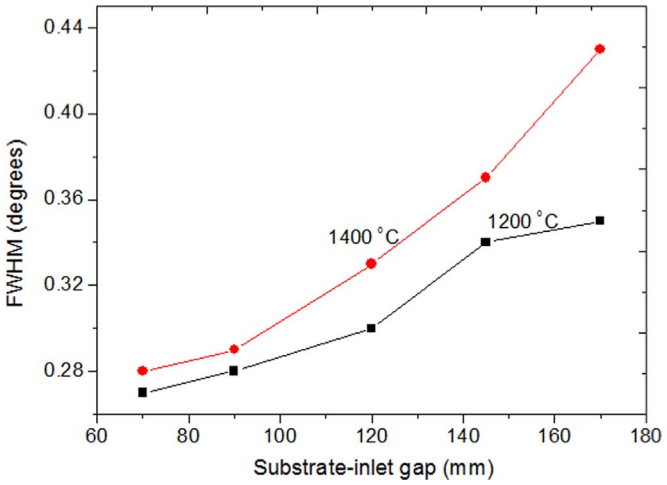

Fig. 8. FWHM of a (200) peak as a function of substrate-inlet gap at 1200 °C and 1400 °C.

3.5. Peak broadening and lattice strain

Fig. 8 shows a plot of the FWHM for the (200) diffraction peak as a function of substrate-inlet gap. From this figure, it is quite clear that the FWHM increases with substrate-inlet gap indicating peak broadening. Broadening of XRD peaks indicates a possible decrease in crystallite size (grain refinement) and/or the presence of lattice strain in the material [32].

Strain is a measure of distortions and crystal imperfections in the material. The strain is calculated from FWHM, denoted by B, and diffraction angle θ using Eq. (13) [33].

$$\varepsilon = \frac{B}{4\tan\theta} \tag{13}$$

The results in Fig. 9 show that as the substrate-inlet gap increases, the strain in the ZrC films increased. The strain in the films is likely to have been introduced in the lattice planes during deposition by chemical and thermal processes. Polycrystalline films deposited on a substrate are usually in a strained state [34]. The increase in strain in the film as the substrate-inlet gap increased may be due to reduced film thickness, decreased reactant concentrations, the effects of crystallite size, and also the increase in impurities (free carbon). Strain causes the

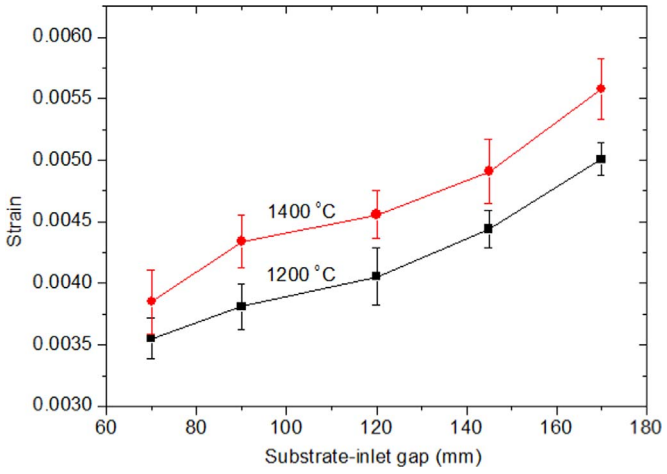

Fig. 9. Effect of substrate-inlet gap on lattice strain at 1200 °C and 1400 °C.

interplanar spacing to change from stress free values to values comparable to the amount of stress introduced [31,35]. A very thin film is likely to be discontinuous [15], introducing stress in the material.

3.6. Preferred orientation

To ascertain whether the crystals displayed preferred orientation, texture coefficients were determined. Texture coefficients $T(hkl)$ are calculated from Eq. (14).

$$T(hkl) = \frac{I(hkl)/I_0(hkl)}{(1/N)\sum_N I(hkl)/I_0(hkl)} \quad (14)$$

where $I(hkl)$ is the relative intensity of the (hkl) plane as measured from the diffraction pattern of the sample and N is the number of diffraction peaks considered. In this case only the first five ZrC reflections of the XRD patterns of each sample were considered (i.e. N=5). The quantity $I_0(hkl)$ is the relative integrated intensity reference of the randomly oriented grains (powder of the sample) [31,36]. The value of $I_0(hkl)$ for the corresponding plane was obtained from the ICDD data file number ZrC: 03-065-8833.

Preferred orientation influences the properties of crystalline materials. Values of the texture coefficient, $T(hkl)$, less or equal to one means that the crystallites are randomly oriented, while a value of $T(hkl)$ greater than one implies preferred orientation of the crystallites in a given hkl direction [36–38]. Figs. 10 and 11 show the variation of texture coefficient with substrate-inlet gap at substrate temperature of 1200 °C and 1400 °C respectively.

At 1200 °C, the texture coefficient is greater than one for all films, implying preferential orientation in all the indicated diffraction planes. The (220) plane is most preferred with a $T(hkl)$ value of 3.6 at 70 mm. At 90 mm and 120 mm, plane (200) was slightly more preferred than (220). There was a general decrease in the $T(hkl)$ values for all the diffraction planes at substrate inlet gaps of 145–170 mm. The diffraction plane (111) was generally the least preferred orientation. This may be due high surface energy and reactant concentration when the substrate-inlet gap is narrowed.

For ZrC films deposited at 1400 °C, the plane (200) was more preferred at 70 mm and 90 mm. When the substrate-inlet gap widened, the preferred orientation shifted to (220). Similar to results at 1200 °C, (111) was the less favoured diffraction plane. This may be due to increased temperature of 1400 °C which increases the surface energy and atomic mobility. However the accumulation of impurities such as free carbon on the substrate surface greatly influences the surface energy.

The degree of preferred orientation (α) of each sample as a whole was determined by the standard deviation (from the powdered sample) of all the values of $T(hkl)$for each sample calculated from Eq. (15).

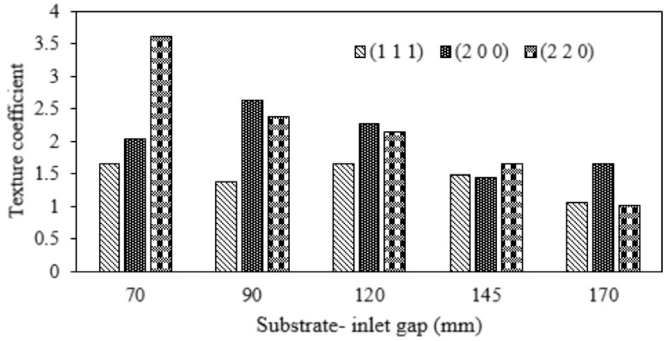

Fig. 10. Texture coefficient of ZrC films deposited at 1200 °C as a function of substrate-inlet gap.

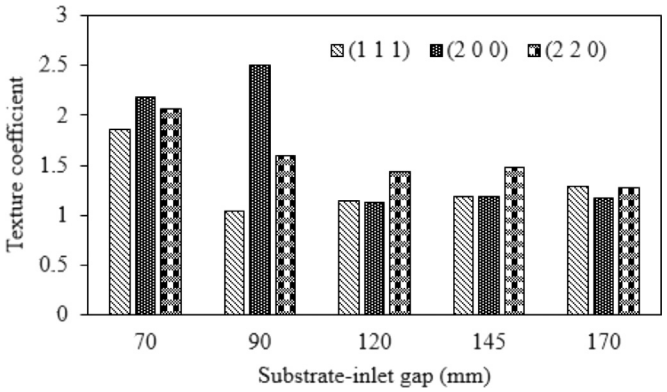

Fig. 11. Texture coefficient of ZrC films deposited at 1400 °C as a function of substrate-inlet gap.

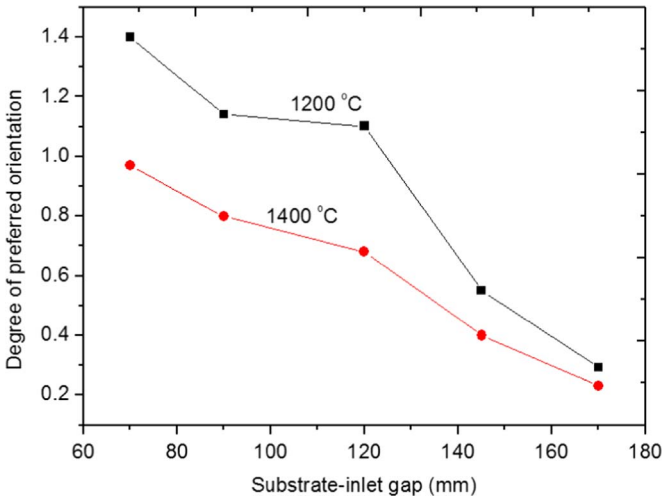

Fig. 12. Effect of substrate-inlet gap on degree of preferred orientation of ZrC films.

$$\alpha = \sqrt{(1/N)\sum_N [T(hkl) - T_o(hkl)]^2} \quad (15)$$

The value of $T_o(hkl)$ is always equal to one since it represents the texture coefficient of the powder of the sample [36,38,39]. Fig. 12 shows the variation of the degree of preferred orientation with substrate-inlet gap. All samples haveα-values greater than zero indicating good degree of preferential orientation at both temperatures. The α-values decreases as the substrate-inlet gap and temperature increases. This indicates that to produce films with highly preferred orientation a relatively narrow substrate-inlet gap is recommended.

3.7. Surface morphology and microstructure

The FE-SEM was used to examine the surface morphology and microstructure of ZrC films. The micrographs of ZrC film surfaces deposited at 1200 °C for different substrate-inlet gaps are depicted in Fig. 13. At 70 mm (Fig. 13(A)), the ZrC film surface show a large complex facetted structure surrounded by small particles existing at the periphery and on top. These small particles have the same shape as the larger ones (see the high magnification insert in Fig. 13(A)). The surface morphology at substrate-inlet gap of 120 mm indicated in Fig. 13(B)) show small granules almost of the same size with very few openings on film surface. These small granules have the same structure (complex facets) as those at 70 mm (see the insert Fig. 13(B)). At 170 mm (Fig. 13(C)), ZrC film surface show ball-shaped particles clustered together forming a cauliflower-like shape. The cauliflower-like clusters of varying sizes are surrounded by numerous large openings, compared to that of the image at 120 mm.

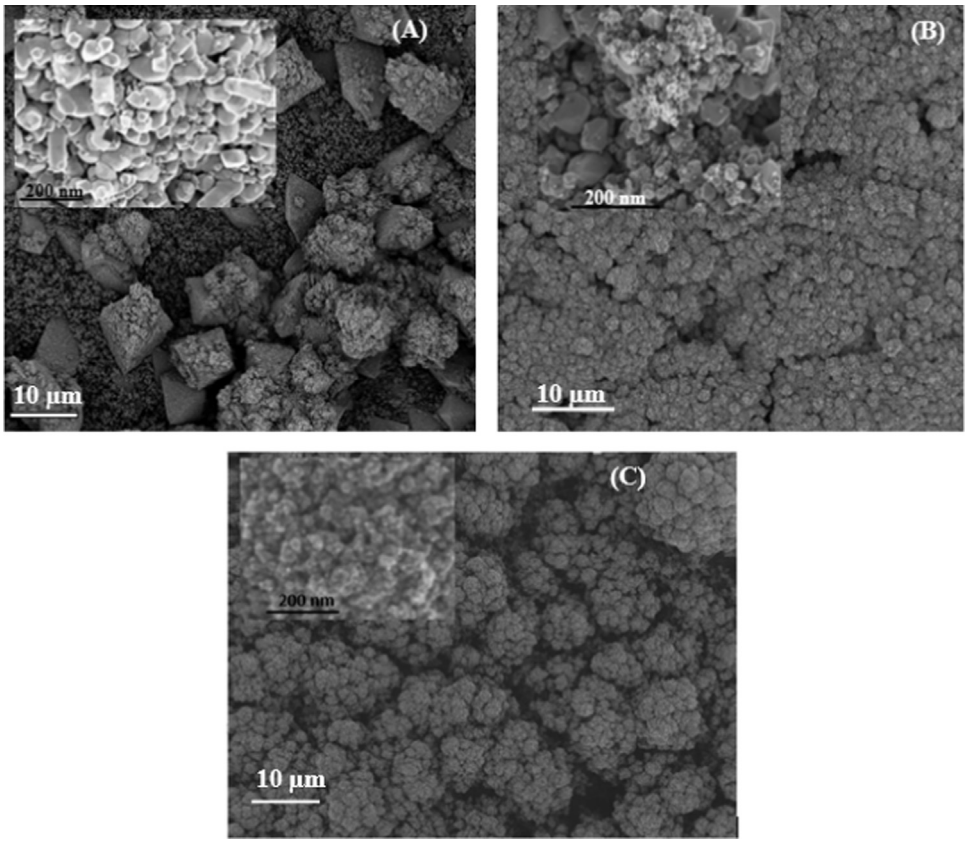

Fig. 13. SEM images of ZrC films deposited at 1200 °C for substrate-inlet gap of (A) 70 mm, (B) 120 mm and (C) 170 mm.

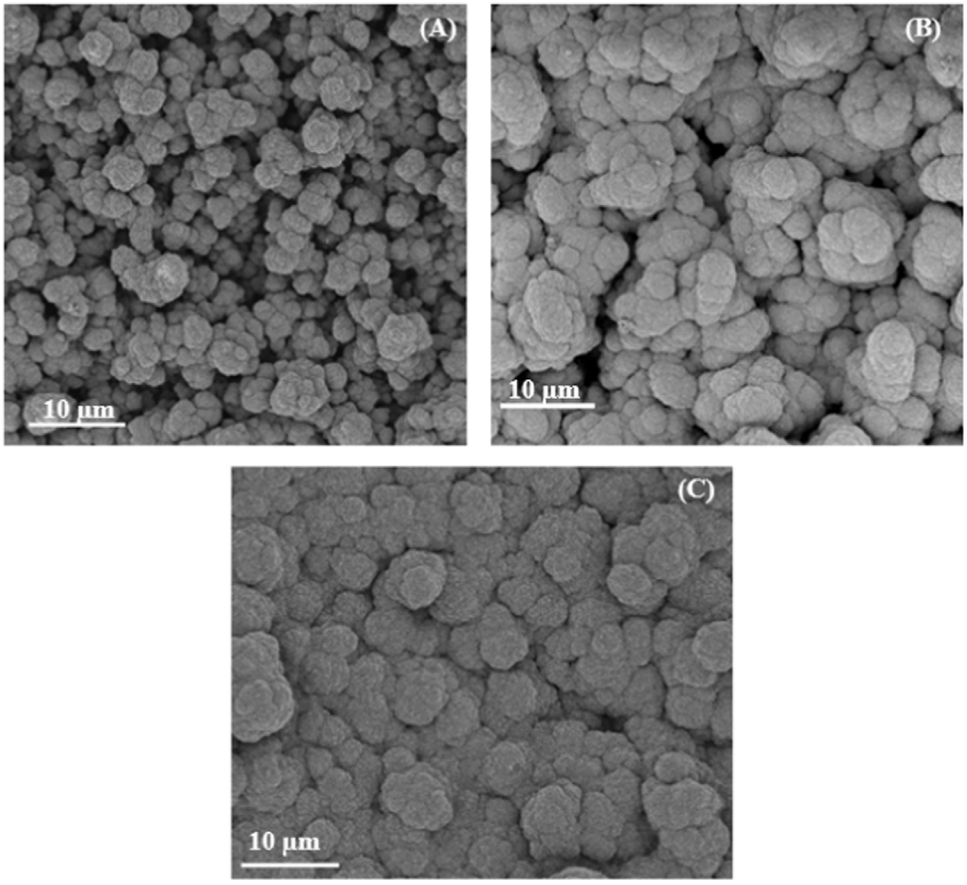

Fig. 14. SEM images of ZrC films deposited at 1400 °C for substrate-inlet gap of (A) 70 mm, (B) 120 mm and (C) 170 mm.

Fig. 14 shows surface morphology of ZrC films deposited at 1400 °C for substrate-inlet gap of 70 mm (Fig. 14(A)), 120 mm (Fig. 14(B)) and 170 mm (Fig. 14(C)). At 70 mm, the surface morphology consists of agglomerates of ball-like particles surrounded by openings. At 120 mm these agglomerates (cauliflower-like) become bigger and the size of the openings surrounding them reduces significantly. As the substrate-inlet gap increases to 170 mm the surface morphology is more uniform, dense and smoother with almost no openings around the clusters. The cauliflower-like clusters tend to pebble-like structure.

The average particle sizes (for the different gap conditions increased for the 1400 °C grown films. This can be attributed to the increase in the surface energy and mobility of the ZrC molecules on the surfaces of the deposited (poly-crystalline) ZrC crystals at the higher temperature. Another reason for the increase in particle size (agglomeration) as substrate-inlet gap increased may be due to the increase in carbon impurities in the films which acts as additional nucleation sites. Judging from these results, it is quite clear that the substrate-inlet gap and substrate temperature controls the morphology and growth uniformity of ZrC films.

4. Conclusion

ZrC films were prepared at atmospheric pressure on graphite substrates in a vertical CVD reactor. $ZrCl_4$-CH_4-H_2-Ar mixtures were used at substrate temperature of 1200 °C and 1400 °C for 2 h. For the deposition of the films in the reactor, the substrate-inlet gap was varied in the range of 70–170 mm. The results showed a higher growth rate for the ZrC films deposited at 1400 °C compared to 1200 °C, and that the growth rate decreased with increasing substrate-inlet gap at both temperatures. The boundary layer thickness increased with increase in the substrate-inlet gap, resulting in lower fluxes and growth rates. The diffusion coefficient of the reactants was found to be 0.176 cm^2/s and 0.200 cm^2/s for growth temperature of 1200 °C and 1400 °C respectively. The diffusion of source materials through the boundary layer to the reacting surface was also illustrated using a model. The XRD results showed the formation of ZrC and some traces of free carbon. The C/ZrC ratio increased with substrate-inlet gap at both temperatures, with 1400 °C having the highest ratio. There was a general decrease in average crystallite size with increasing substrate-inlet gap at both deposition temperatures. The lattice strain increased with substrate-inlet gap; this may be due to increase in lattice imperfection resulting from increased concentration of free carbon. The diffraction plane (111) was the less favoured orientation, whereas (200) and (220) were more favoured planes. The degree of preferred orientation decreased with substrate-inlet gap at the two temperatures. The samples deposited at 1200 °C had a higher degree of orientation than those deposited at 1400 °C. For the 1200 °C substrate temperature, at a 70 mm substrate-inlet gap, the crystals had better developed facets with high crystallinity which deteriorated with increase in substrate-inlet gap. At 1400 °C, as the substrate-inlet gap was increased from 70 to 170 mm, the cauliflower-like structure became more uniform with increasing particle agglomeration.

Acknowledgements

The authors would like to acknowledge University of Pretoria, Busitema University and African Union for financial support. Necsa and the Department of Science and Technology of South Africa through the Nuclear Materials Development Network of the Advanced Metals Initiative is highly appreciated for the provision of laboratory space and experimental materials.

References

[1] H.O. Pierson, Handbook of Refractory Carbides and Nitrides: Properties, Characteristics, Processing and Apps, William Andrew, New Jersey, United States, 1996.
[2] M.K. Meyer, R. Fielding, J. Gan, Fuel development for gas-cooled fast reactors, J. Nucl. Mater. 371 (2007) 281–287.
[3] Y. Katoh, G. Vasudevamurthy, T. Nozawa, L.L. Snead, Properties of zirconium carbide for nuclear fuel applications, J. Nucl. Mater. 441 (2013) 718–742.
[4] D.J. Varacalle, L.B. Lundberg, H. Herman, G. Bancke, W.L. Riggs, Vacuum plasma sprayed zirconium carbide coatings, Surf. Coat. Technol. 68 (1994) 86–91.
[5] M. Dollé, D. Gosset, C. Bogicevic, F. Karolak, D. Simeone, G. Baldinozzi, Synthesis of nanosized zirconium carbide by a sol-gel route, J. Eur. Ceram. Soc. 27 (2007) 2061–2067.
[6] C. Ang, T. Williams, A. Seeber, H. Wang, Y.-B. Cheng, Synthesis and evolution of zirconium carbide via sol-gel route: features of nanoparticle oxide-carbon reactions, J. Am. Ceram. Soc. 96 (2013) 1099–1106.
[7] M.D. Sacks, C.-A. Wang, Z. Yang, A. Jain, Carbothermal reduction synthesis of nanocrystalline zirconium carbide and hafnium carbide powders using solution-derived precursors, J. Mater. Sci. 39 (2004) 6057–6066.
[8] C.-S. Chen, C.-P. Liu, C.-Y. Tsao, Influence of growth temperature on microstructure and mechanical properties of nanocrystalline zirconium carbide films, Thin Solid Films 479 (2005) 130–136.
[9] X. Yang, Z. Su, Q. Huang, L. Chai, P. Zhong, L. Xue, A zirconium carbide coating on graphite prepared by reactive melt infiltration, J. Cent. South Univ. 21 (2014) 472–476.
[10] Q. Liu, L. Zhang, L. Cheng, Y. Wang, Morphologies and growth mechanisms of zirconium carbide films by chemical vapor deposition, J. Coat. Technol. Res. 6 (2009) 269–273.
[11] K. Ikawa, Vapor deposition of zirconium carbide-carbon composites by the chloride process, J. Less Common Met. 29 (1972) 233–239.
[12] J. Gyu, S. Jung, J. Yeon, D. Jin, The effect of temperature on the growth and properties of chemical vapor deposited ZrC films on SiC-coated graphite substrates, Ceram. Int. 41 (2015) 211–216.
[13] X.-T. Yan, Y. Xu, Chemical vapour deposition: an integrated engineering design for advanced materials, Springer Science & Business Media, London, 2010.
[14] K.L. Choy, Chemical vapour deposition of coatings, Prog. Mater. Sci. 48 (2003) 57–170.
[15] S. Franssila, Introduction to Microfabrication, John Wiley & Sons, Chichester, England, 2010.
[16] S.P. Vanka, G. Luo, N.G. Glumac, Parametric effects on thin film growth and uniformity in an atmospheric pressure impinging jet CVD reactor, J. Cryst. Growth 267 (2004) 22–34.
[17] S. Biira, P.L. Crouse, H. Bissett, B.A.B. Alawad, T.T. Hlatshwayo, J.T. Nel, J.B. Malherbe, Optimisation of the synthesis of ZrC coatings in an RF induction-heating CVD system using surface response methodology, Thin Solid Films (2016) Submitted.
[18] A.X.S.Bruker, TOPAS, Version 4.2, Bruker AXS, Karlsruhe, Ger, 2009.
[19] H.O. Pierson, Handbook of Chemical Vapor Deposition: Principles, Technology and Applications, William Andrew, New Jersey, United States, 1999.
[20] E.L. Cussler, Diffusion: Mass Transfer in Fluid Systems, Cambridge University Press, Cambridge, United Kingdom, 2009.
[21] P.M. Martin, Handbook of Deposition Technologies for Films and Coatings: Science, Applications and Technology, William Andrew, Boston, New York, 2009.
[22] C. Li, L. Huang, G.P. Snigdha, Y. Yu, L. Cao, Role of boundary layer diff usion in vapor deposition growth of chalcogenide nanosheets: the case of GeS, ACS Nano 6 (2012) 8868–8877.
[23] M.S. Kim, J.S. Chun, Effects of the experimental conditions of chemical vapour deposition on a TiC/TiN double-layer coating, Thin Solid Films 107 (1983) 129–139.
[27] S.K. Ghandhi, R.J. Field, A re-examination of boundary layer theory for a horizontal CVD reactor, J. Cryst. Growth 69 (1984) 619–622.
[29] W.K. Burton, N. Cabrera, F.C. Frank, The growth of crystals and the equilibrium structure of their surfaces, Philos. Trans. R. Soc. Lond. A Math. Phys. Eng. Sci. 243 (1951) 299–358. http://dx.doi.org/10.1098/rsta.1948.0007.
[30] M.Ermrich, D.Opper, XRD for the analyst: getting acquainted with the principles, PANalytical, 2013.
[31] B.D. Cullity, S.R. Stock, Elements of X-ray Diffraction, Pearson, Massachusetts, United States, 2001.
[32] K. Venkateswarlu, A.C. Bose, N. Rameshbabu, X-ray peak broadening studies of nanocrystalline hydroxyapatite by Williamson-Hall analysis, Phys. B Condens. Matter 405 (2010) 4256–4261.
[33] V.D. Mote, Y. Purushotham, B.N. Dole, Williamson-Hall analysis in estimation of lattice strain in nanometer-sized ZnO particles, J. Theor. Appl. Phys. 6 (2012) 1–8.
[34] G. Janssen, Stress and strain in polycrystalline thin films, Thin Solid Films 515 (2007) 6654–6664.
[35] R. Sharma, D.P. Bisen, U. Shukla, B.G. Sharma, X-ray diffraction: a powerful method of characterizing nanomaterials, Recent Res. Sci. Technol. 4 (2012) 77–79.
[36] J.P. Enríquez, X. Mathew, Influence of the thickness on structural, optical and electrical properties of chemical bath deposited CdS thin films, Sol. Energy Mater. Sol. Cells 76 (2003) 313–322.
[37] S. Aksoy, Y.Y. Caglar, S. Ilican, M. Caglar, Effect of deposition temperature on the crystalline structure and surface morphology of ZnO films deposited on p-Si, Adv. Control. Chem. Eng. Civ. Eng. Mech. Eng. (2010) 227–231.
[38] H.R. Moutinho, F.S. Hasoon, F. Abulfotuh, L.L. Kazmerski, Investigation of polycrystalline CdTe thin films deposited by physical vapor deposition, close-spaced sublimation, and sputtering, J. Vac. Sci. Technol. A. 13 (1995) 2877–2883.
[39] K.H. Kim, J.S. Chun, X-ray studies of SnO2 prepared by chemical vapour deposition, Thin Solid Films 141 (1986) 287–295.